1996ApJ...459..156M

THE ASTROPHYSICAL JOURNAL, 459:156–168, 1996 March 1
© 1996. The American Astronomical Society. All rights reserved. Printed in U.S.A.

SIMULTANEOUS SOFT X-RAY AND GeV GAMMA-RAY OBSERVATIONS OF BL LACERTAE OBJECT AO 0235+164

GREG MADEJSKI,[1,2] TADAYUKI TAKAHASHI,[3,4] MAKOTO TASHIRO,[3] HIDETOSHI KUBO,[3]
ROBERT HARTMAN,[1] TIMOTHY KALLMAN,[1] AND MAREK SIKORA[1,5,6]
Received 1995 June 27; accepted 1995 September 1

ABSTRACT

We present data collected during a simultaneous GeV γ-ray (*Compton Gamma Ray Observatory* EGRET) and X-ray (*ASCA*) observation of BL Lac object AO 0235+164 ($z = 0.94$); we also present *ROSAT* PSPC X-ray data, obtained 6 months earlier. The X-ray spectra from both *ROSAT* and *ASCA* confirm a substantial photoelectric absorption beyond the value expected from our Galaxy, which is most likely caused by heavy elements in the inerstellar medium of an intervening galaxy at $z = 0.524$; it is possible to measure the elemental abundances in it modulo the hydrogen spin temperature T_S. By comparing the absorption in our data to the 21 cm absorption, we can limit T_S to at most $\sim$700 K.

The *ROSAT* data imply a rapid ($\sim$3 day) doubling of the soft X-ray flux and a subsequent quasi-exponential decay, whereas no variability is apparent in the *ASCA* or EGRET data. We detect a significant spectral change of the BL Lac X-ray continuum between the *ROSAT* and *ASCA* observations; *ASCA* data show that the spectrum is substantially harder (with the energy power-law index $\alpha \sim 1$ vs. ~ 2) and fainter than in the *ROSAT* data. The simplest interpretation of this spectral variability is that the *ROSAT* data are dominated by a bright, soft tail of a synchrotron component, which disappeared during the *ASCA* observation, uncovering a harder Compton component.

The EGRET data imply a lower GeV flux than in the previous observations, with no apparent change of the GeV spectrum. The ratio of the γ-ray to the X-ray flux [in $E \times F(E)$] for this radio-discovered object is roughly 30, which is very substantially higher than that inferred for X-ray–discovered BL Lac objects, suggesting an important difference in the structure between the two subclasses of BL Lac objects.

Subject headings: BL Lacertae objects: individual (AO 0235+164) — gamma rays: observations — X-rays: galaxies

1. INTRODUCTION

AO 0235+164, one of the "original" BL Lac objects, was discovered on the basis of the optical identification of a variable radio source by Spinrad & Smith (1975); its redshift (inferred from weak emission lines) is 0.94 (Cohen et al. 1987). It is one of the most optically variable BL Lac objects, varying by a factor of 100 (Rieke et al. 1976). Importantly, *Compton Gamma Ray Observatory* EGRET data show strong GeV γ-ray emission (Hunter et al. 1993), with a flux variable from observation to observation (von Montigny et al. 1995); no rapid (timescale less than $\sim$1 week) GeV variability has been reported, but this may be attributable to sparse sampling. AO 0235+164 has all the characteristics of optically violent variable (OVV) quasars (including the GeV emission), except that it shows only very weak optical emission lines, and as such, it may be an intermediate object between the two subclasses of a larger class called "blazars;" true, lineless BL Lac objects and OVVs.

High-resolution optical spectroscopy revealed two absorption-line systems, one at $z_{ab1} = 0.524$ and a weaker one at $z_{ab2} = 0.852$ (Burbidge et al. 1976; Rieke et al. 1976). The sysem at $z_{ab1} = 0.524$ is also observed in 21 cm absorption (Roberts et al. 1976; Wolfe & Wills 1977). Historically, the absorption data added to the body of evidence for the extragalactic nature of BL Lac objects, and by extension, radio-loud quasars. It was speculated that the location of this object behind a galaxy could explain the variability as a result of gravitational microlensing (Ostriker & Vietri 1985), although this has been disputed recently (Abraham et al. 1993; see also Wolfe, Davis, & Briggs 1982). Nonetheless, the column density of the absorbing material, as inferred from the ground-based observations, should be sufficient, under reasonable cosmic abundances, to show up as photoelectric absorption in the X-rays. Indeed, the previous data (from the *Einstein Observatory* Imaging Proportional Counter, or the IPC) showed such absorption, at a level significantly greater than expected from our own Galaxy (Madejski 1994). Since the *IUE* UV data (Snijders et al. 1982) imply that the hydrogen column density in that system at $z_{ab2} = 0.852$ is at most 10^{17} cm^{-2}, several orders of magnitude lower than the $z_{ab1} = 0.524$ system, we can safely assume that such absorption is entirely dominated by the latter; this is further supported by a nondetection of the 21 cm absorption redshifted to $z = 0.852$. With the optical and radio data available, the X-ray absorption should yield elemental abundances in the intervening galaxy, although it is important to note that the $z = 0.524$ system is unusual in its own right, showing strong emission lines *without* a bright nuclear source, and it may not be representative of ordinary galaxies (Cohen et al. 1987).

The goal of the observations reported here was therefore twofold: one was to measure precisely the soft X-ray spectrum, in order to study the details of the photoelectric absorption of the intervening system. The other was to

[1] Laboratory for High Energy Astrophysics, Code 666, NASA/Goddard Space Flight Center, Greenbelt, MD 20771.
[2] With Universities Space Research Association.
[3] Physics Department, University of Tokyo, 7-3-1, Hongo, Bunkyo-ku, Tokyo 113, Japan.
[4] Institute of Space and Astronautical Science, 3-1-1 Yoshinodai, Sagamihara, Kanagawa, 299, Japan.
[5] Copernicus Center, ul. Bartycka 18, 00-716, Warsaw, Poland.
[6] JILA/University of Colorado, Boulder, CO.

© American Astronomical Society • Provided by the NASA Astrophysics Data System

1996ApJ...459..156M

obtain the X-ray and γ-ray data *simultaneously*, to determine the relationship of the X-ray spectrum to the GeV spectrum, which is important for modeling of the overall electromagnetic emission from this highly variable object. We note here that the source was a subject of a multiwavelength ground-based campaign coincident with the *GRO* and *ASCA* observations, but the results from other wavelengths will be reported elsewhere. We present the *ROSAT*, *ASCA*, and EGRET data in § 2, show the spectral fits in § 3, and discuss the X-ray absorption and overall X-ray to γ-ray spectrum in § 4.

2. OBSERVATIONS

2.1. *ROSAT Observations*

AO 0235+164 was observed nine times by *ROSAT* PSPC between 1993 July 21 and 1993 August 15, roughly every 3 days, with each exposure lasting from $\sim$1200 to $\sim$4100 s. The log of the *ROSAT* observations is given in Table 1. The data were processed using SASS version 6.4. The source was clearly detected in each exposure, with a position derived from the summed data at R.A. (2000.0) = $02^h38^m39^s.0$, decl. (2000.0) = 16°37′05″. This is within 10″ of the radio position [R.A. (2000.0) = $02^h38^m38^s.4$, decl. (2000.0) = 16°37′02″], consistent with the *ROSAT* absolute pointing determination. No other sources brighter than 1/10 of the count rate of AO 0235+164 were detected in the image.

The pulse-height analyzer (PHA) X-ray spectrum of the source was derived from the PSPC data in a standard manner, specifically by extracting counts from a circular region 3′.75 in diameter and the background counts from an annulus centered on the source, of inner diameter of 6′.25 and outer diameter of 10′, avoiding any obvious point sources. Only PSPC channels 12 through 211 were used, corresponding to a nominal energy range of 0.1–2.1 keV. For the spectral fitting, we binned the data using five original channels to a bin. The background-subtracted counting rates for each exposure are listed in Table 1.

It is clear from Table 1 that the source flux varied significantly from one exposure to another, with the highest count rate 4.7 times that of the lowest. The light curve of the source is shown in Figure 1*a*. The shape of the light curve is that of a rapid rise (which cannot be resolved with these data) and a more gradual decay. To assure that the variability is not a result of instrumental effects, we measured the background count rate, normalized to a detection cell used for the source spectrum. This was relatively constant from one exposure to another, never reaching more than 12% of

TABLE 1

SUMMARY OF THE *ROSAT* AND *ASCA* OBSERVATIONS OF AO 0235+164

Exposure Name	Observation Start Time (UT)	"On-Source" Time (s)	Net Source Counting Rate	Background Counting Rate (in a Detection Cell)	Net Soft/Hard Count Rate Ratio (rate < 1 keV/rate > 1 keV)
			A. *ROSAT* PSPC Data		
R1	1993 Jul 21 05:32	2083	0.201 ± 0.010	0.0069	0.81 ± 0.083
R2	1993 Jul 24 02:00	1903	0.359 ± 0.014	0.0074	0.96 ± 0.075
R3	1993 Jul 26 19:18	1508	0.287 ± 0.014	0.0102	0.88 ± 0.087
R4	1993 Jul 29 14:14	1192	0.175 ± 0.013	0.0108	0.90 ± 0.133
R5	1993 Aug 1 09:12	1783	0.143 ± 0.010	0.0084	1.02 ± 0.134
R6	1993 Aug 4 08:52	2023	0.118 ± 0.008	0.0143	0.93 ± 0.132
R7	1993 Aug 6 21:56	4099	0.101 ± 0.005	0.0086	0.98 ± 0.102
R8	1993 Aug 12 11:42	1664	0.093 ± 0.008	0.0068	0.94 ± 0.163
R9	1993 Aug 15 08:10	1708	0.077 ± 0.007	0.0055	0.72 ± 0.141
Total ROSAT		17963	0.166 ± 0.0032		
			B. *ASCA* Data		
A1:					
GIS2	1994 Feb 4 19:33	11858	0.021 ± 0.0026		
GIS3		11858	0.029 ± 0.0028		
SIS0		11164	0.038 ± 0.0052		
SIS1		10664	0.032 ± 0.0055		
A2:					
GIS2	1994 Feb 11 22:36	12383	0.023 ± 0.0027		
GIS3		12334	0.028 ± 0.0026		
SIS0		10930	0.041 ± 0.0053		
SIS1		10406	0.302 ± 0.0056		
A3:					
GIS2	1994 Feb 16 01:25	11592	0.018 ± 0.0027		
GIS3		11592	0.028 ± 0.0028		
SIS0		10189	0.037 ± 0.0056		
SIS1		9939	0.028 ± 0.0058		
A4:					
GIS2	1994 Feb 19 03:55	12399	0.023 ± 0.0026		
GIS3		12397	0.030 ± 0.0027		
SIS0		12146	0.041 ± 0.0048		
SIS1		11725	0.038 ± 0.0050		
Total:					
GIS2		48232	0.0214 ± 0.0009		
GIS3		48181	0.0286 ± 0.0010		
SIS0		44429	0.0385 ± 0.0016		
SIS1		42734	0.0322 ± 0.0016		

© American Astronomical Society • Provided by the NASA Astrophysics Data System

1996ApJ...459..156M

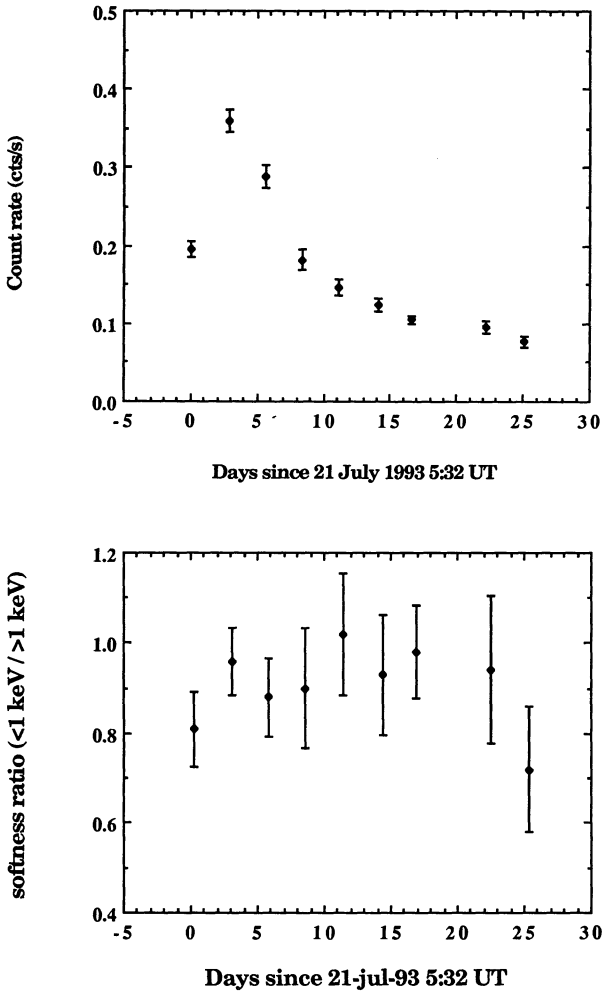

FIG. 1.—The light curve (*top*) and softness ratio (*bottom*) for the *ROSAT* observations of AO 0235+164, clearly showing the flux variability.

the source counting rate (see Table 1). We also examined individual exposures and discovered no significant count rate variability within each exposure.

We examined the data to check if the variability is preferentially attributable to soft or hard photons within the *ROSAT* bandpass. To that end, we considered the photons below and above the nominal channel boundary of 1.0 keV and plotted the ratio of soft to hard count rates in Figure 1*b*. While there is no obvious trend, the lowest flux point also corresponds to the hardest spectrum, but we do not consider this significant.

2.2. *ASCA Data*

ASCA observed AO 0235+164 four times, starting on 1994 February 4, with each exposure lasting ~11,000 s. The four observations (see Table 1) were spaced between 3 and 7 days apart, with the last exposure (1994 February 19) overlapping with the EGRET observation. (The *ASCA* exposures were designed to be fully overlapping with the EGRET pointing, but this was precluded by an EGRET target of opportunity.) *ASCA* consists of four X-ray telescopes, with two having Gas Imaging Spectrometers (GIS2 and GIS3) and two having X-ray sensitive CCDs (known as SIS0 and SIS1) in the focal planes. All observations were performed in one-CCD mode, in the standard spectroscopy configuration. The data were selected using the fairly conservative screening criteria. These include the following: data were accepted when source was farther than 20° from the Earth limb during the orbit day and farther than 5° (GIS) and 10° (SIS) during the orbit night; data were rejected within the South Atlantic Anomaly (SAA) and within 60 s of the crossing of the SAA boundary; data were rejected in the regions with geomagnetic rigidity <6 GeV/c. The source was significantly detected in each exposure in all four detectors; the total "on source" time ranged from about 42 ks to about 48 ks. All data presented here were analysed in the highest resolution "faint" mode, to assure that there would be no additional gain offset from the potential contamination by the scattered sunlight; however, there was no discernible difference between the results of the "faint" and "bright" mode analyses.

The source counts were extracted from each image using a circular region of 6′ diameter for the SIS and 8′ diameter for the GIS data; we used somewhat smaller regions than the standard values to minimize the contamination of these faint source counts by the background. The background was extracted from source-free regions of the same image as the source. For that, we used a region of the same area as the source region for the SISs, and 4 times greater area for the GISs. The resulting spectra from SIS0, SIS1, and GIS2 were then binned in groups of two, four, eight, or 16 original PHA channels to a bin, such that there would be at least ~20 counts per bin. Owing to an on-board electronics malfunction in the GIS3, where the two least significant bits of the analog-to-digital converter in the pulse height discriminator circuit were stuck in a fixed pattern, al data for GIS3 needed to be binned with at least eight channels to a bin. The background-subtracted counting rates are given in Table 1. In contrast to the *ROSAT* observation, there is no variability from one *ASCA* exposure to another. Thus, we extracted a summed spectrum from the entire *ASCA* observation.

2.3. *Compton GRO EGRET Observations*

EGRET observed AO 0235+164 starting on 1994 February 17. The total exposure lasted for 2 weeks. At $E > 100$ MeV, the source was detected at the level of 14×10^{-8} photons cm^{-2} s^{-1}, which is a 3 σ detection. This is significantly lower than measured by the original discovery observation (Hunter et al. 1993), and in fact it was the lowest of all measurements of the source to date (von Montigny et al. 1995). Even though it was not possible to derive good limits on the source spectrum, in Figure 7 we plot the EGRET data in the $E \times F(E)$ versus E representation in two energy bands, 0.3–1 GeV and 1–10 GeV, with the associated error bars on flux measurement. Even though in each of these bands the source was detected only at 2.2 and 2.7 σ, respectively, the purpose of plottting two separate energy channels in this figure is to illustrate that the EGRET data are consistent with a power-law spectrum with $\alpha = 1.0$, reported by Hunter et al. (1993); such a spectrum would appear as a flat line in that figure. With an assumed $\alpha = 1.0$, we infer a 1 GeV flux density [in $E \times F(E)$] of 0.014 keV cm^{-2} s^{-1}.

3. SPECTRAL FITTING

3.1. *ROSAT Spectrum*

Since each *ROSAT* exposure did not produce enough source counts to yield a meaningful measurement of the

© American Astronomical Society • Provided by the NASA Astrophysics Data System

1996ApJ...459..156M

spectrum, and there was no obvious change in the ratio of soft to hard count rates as a function of the source flux, we used summed *ROSAT* data in the subsequent spectral fitting; the mean background-subtracted counting rate was 0.17 counts s^{-1}. We fitted them to a simple, absorbed power-law model, using the cross sections as given by Morrison & McCammon (1983, hereafter MMC83). The fit is acceptable ($\chi^2 = 30.2/40$ PHA bins), with best-fit parameters $\alpha = 2.03^{+0.50}_{-0.45}$, and $N_H = 3.0^{+0.8}_{-0.7} \times 10^{21}$ cm^{-2}; all spectral fits are tabulated in Table 2. (Throughout this paper, we use the energy power-law index α, defined via flux density $F_E = F_o E^{-\alpha}$, and we quote all errors as corresponding to 90% confidence contours for a single interesting parameter, i.e., $\chi^2 + 2.7$.) We show the data and corresponding residuals in Figure 2. This value of the fitted column density is substantially larger than the Galactic value of 7.6×10^{20} cm^{-2} (determined using 21 cm data; Elvis, Lockman, & Wilkes 1989). As we argue in § 4.1.1, the absorption above the Galactic value is likely to arise in the intervening galaxy at $z = 0.524$. Therefore, we also fit the data to a model consisting of a power law, a fixed absorbing column density of 7.6×10^{20} cm^{-2}, and an additional MMC83 absorber at $z = 0.524$. (We note here that the use of the redshifted MMC83 absorber in this case is likely *not* to be appropriate, and we return to this point in § 4.1.) The excess absorption is now $3.8^{+1.2}_{-1.1} \times 10^{21}$ cm^{-2}, and the power-law index α is $1.67^{+0.32}_{-0.32}$, with $\chi^2 = 27.4/40$ PHA bins. Using either spectrum, the 0.5–2 keV flux ranges from 0.8 to 3.6×10^{-12} ergs cm^{-2} s^{-1}, with a mean value of 1.7×10^{-12} ergs cm^{-2} s^{-1}; the mean unabsorbed 1 keV flux density is 1.24 μJy.

3.2. *ASCA Spectrum*

Since the source showed essentially no variability during the four *ASCA* exposures, the *ASCA* data from all four observations for each detector were summed and fitted in an analogous manner to the *ROSAT* data. We fitted data from all four detectors simultaneously, allowing each normalization to be free, to allow for residual calibration uncertainties. A simple, absorbed power-law model (with all absorption at $z = 0$) yielded an acceptable fit (χ^2 of 341 for 354 PHA channels) with an index $\alpha = 1.01^{+0.09}_{-0.10}$ and column density of $2.7 \pm 0.5 \times 10^{21}$ cm^{-2}. The data and corresponding residuals for the GIS2 detector are shown in Figure 3; other detector data look similar. Again, requiring that a fixed amount of absorption corresponding to

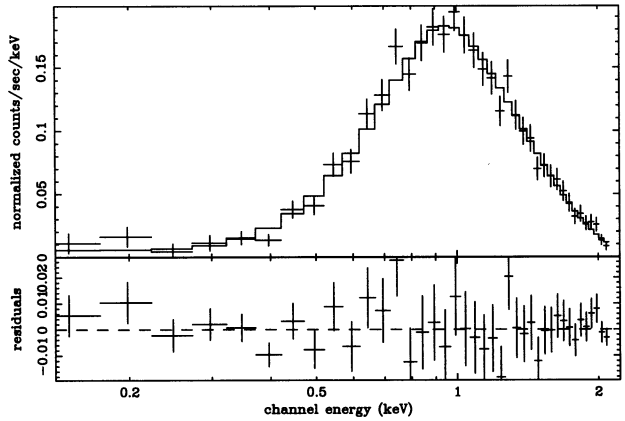

FIG. 2.—The data (*top*) and residuals (*bottom*) for the summed *ROSAT* observation of AO 0235+164, fitted to a power-law model, absorbed by a gas with abundances and cross sections given by Morrison & McCammon, located at $z = 0$.

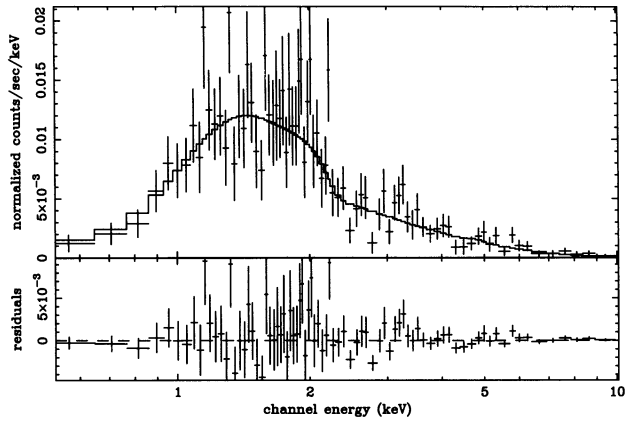

FIG. 3.—The data (*top*) and residuals (*bottom*) for the summed GIS2 data for the *ASCA* observations of AO 0235+164, fitted to a power-law model, absorbed by a gas with abundances and cross sections given by Morrison & McCammon, located at $z = 0$.

7.6×10^{20} cm^{-2} is attributable to our Galaxy, and allowing the excess absorption to be located at $z = 0.524$, with the same caveat as in the previous section, we find that the excess is $4.6^{+1.3}_{-1.3} \times 10^{21}$ cm^{-2}, with the corresponding energy power-law index $\alpha = 0.96 \pm 0.09$. Using either spectrum, the observed 0.5–2 keV flux is 0.4×10^{-12} ergs cm^{-2} s^{-1}, with the unabsorbed 1 keV flux density of 0.3 μJy.

Even though we do not expect that an Fe K line would be detected from the BL Lac object, nonetheless we searched our data for limits on such a line, as it may be present in the intervening galaxy. Depending on the ionization stage of Fe, it would be expected at 4.2–4.7 keV at $z = 0.524$; a detection of such a line would be an indication that the intervening system is indeed an active galactic nucleus (AGN) with a strong X-ray emission, and that our X-ray spectrum of the BL Lac object may be contaminated by a contribution from it. In order to determine the possible strength of such a line, we added a Gaussian line with an assumed width (σ) of 100 eV to the model with absorption at $z = 0.524$, and we measured the resulting χ^2 as a function of the line energy in the interval between 4 and 5 keV. We determined that no significant line is present there, with 90% confidence limit on the line equivalent width of ~60 eV. The limits on the line strength if emitted at $z = 0.94$ (and observed between 3 and 4 keV) are somewhat larger, ~100 eV.

3.3. *Joint ROSAT-ASCA Spectral Fits*

A comparison of the *ROSAT* and *ASCA* data indicates clearly that while the X-ray absorption is consistent between the two data sets, the power-law index has changed significantly. That is best illustrated in Figure 4, where on the same panel, we show the confidence contours for the *ROSAT* and *ASCA* data. Quantitatively, the value of χ^2 for a fit to both data sets with the same power law and absorption (at $z = 0$), but free normalizations, is 431, versus 371 if we allow separate power-law indices for the two data sets (see Table 2). Could the difference in index be only related to the different bandpasses of *ROSAT* and *ASCA*? Of course, it is the low-energy end of the combined spectrum that is sensitive to absorption, while the high end is sensitive to the underlying continuum. To test this, we restricted the *ASCA* bandpass to extend only to 2 keV and repeated the spectral fits (see Table 2). The spectral index is now $\alpha = 0.72^{+0.42}_{-0.43}$, well within 90% confidence regions of the full-bandpass *ASCA* index, and significantly different than the

© American Astronomical Society • Provided by the NASA Astrophysics Data System

© American Astronomical Society • Provided by the NASA Astrophysics Data System

TABLE 2

SPECTRAL FITS TO THE *ASCA* AND *ROSAT* DATA FOR AO 0235+164

	Power Law Plus Free Absorption at $z = 0$			Power Law Plus Galactic Absorption at $z = 0$ Plus Free Absorption at $z = 0.524$			
Data Set	Power-Law Energy Index	Absorption ($\times 10^{21}$ cm^{-2})	χ^2/Number of PHA Channels	Power-Law Energy Index	Galactic Absorption ($\times 10^{21}$ cm^{-2}) (fixed)	$z = 0.524$ Absorption ($\times 10^{21}$ cm^{-2})	χ^2/Number of PHA Channels
Data Sets Fitted Separately							
ROSAT	2.03 (+0.50, −0.45)	3.0 (+0.8, −0.7)	30.2/40	1.67 (+0.32, −0.32)	0.76	3.8 (+1.2, −1.1)	27.4/40
ASCA 0.5–10 keV	1.01 (+0.09, −0.10)	2.75 (+0.51, −0.47)	341/354	0.96 (+0.09, −0.09)	0.76	4.6 (+1.3, −1.3)	340/354
ASCA 0.5–2 keV	0.72 (+0.42, −0.43)	2.2 (+0.9, −1.0)	155/165	0.61 (+0.30, −0.31)	0.76	2.8 (+1.9, −1.6)	151/165
Data Sets Fitted Together[a]							
ROSAT	1.92 (+0.25, −0.27)	2.82 (+0.40, −0.41)	...	1.77 (+0.25, −0.23)	0.76	4.15 (+0.92, −0.84)	...
ASCA	1.02 (+0.08, −0.08)	2.82 (+0.40, −0.41)	371/394	0.93 (+0.08, −0.07)	0.76	4.15 (+0.92, −0.84)	368/394

NOTES.—All errors are 90% confidence regions ($\chi^2 + 2.7$).

[a] The joint fit assumed that the absorption between the *ROSAT* and *ASCA* data sets are the same, but the power-law index was allowed to vary between the two data sets. Note that this is equivalent to a "soft excess" model parameterized as a broken power law, with the energy of the break varying from the *ROSAT* to the *ASCA* observation epochs.

1996ApJ...459..156M

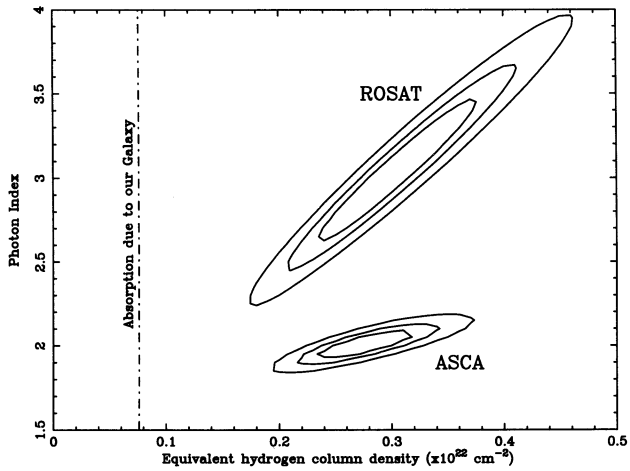

FIG. 4.—Confidence contours (χ^2 + 2.3, 4.6, and 9.2) on the absorbing column density (at $z = 0$) and power-law index for *ROSAT* data (*upper contours*) and *ASCA* data (*lower contours*). The comparison of the two data sets clearly indicates index variability but no absorption variability. The absorption is clearly in excess of the Galactic value of 7.6×10^{20} cm^{-2}.

ROSAT index. Thus, we conclude that the spectral variability is *not* just an artifact of the difference between the *ROSAT* and *ASCA* bandpasses.

It is possible that our assumed spectral form, an absorbed power law, is too simple of a shape to describe adequately the spectrum observed with the two satellites? Since the spectrum appears to be softer in the *ROSAT* observation, we investigated if the true spectral shape could be a hard power law with a "soft excess" of flux above the hard power law extrapolated to lower energies. To that end, we attempted a broken power-law spectrum, described by one index α_{lo} below some break energy E_b, and by another index α_{hi} above E_b. First we considered the *ROSAT* and *ASCA* data separately. Individual fits to the *ROSAT* data yielded a marginal reduction of total value of χ^2 (with $\Delta\chi^2$ of 1.6 for the absorber at $z = 0$ and 1.1 for the absorber at $z = 0.524$, respectively), but with the addition of two free parameters, the χ^2/degrees of freedom is actually worse. Similarly, we adopted such a broken power-law model for the *ASCA* data, which yielded $\Delta\chi^2$ of 1.0 for the absorber at $z = 0$ and 2.9 for the absorber at $z = 0.524$.

We also attempted a broken power-law fit to the combined *ROSAT* and *ASCA* data sets. As above, we adopted

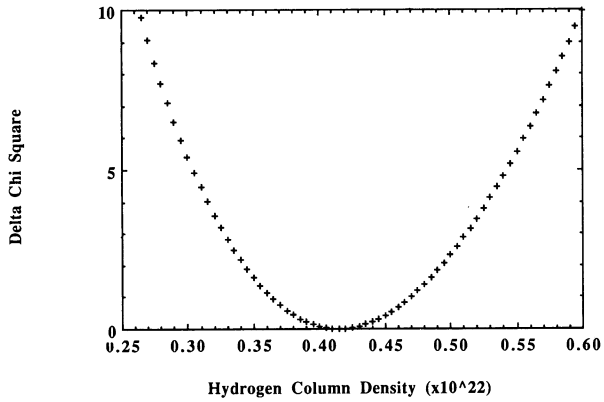

FIG. 5.—$\Delta\chi^2$ (as compared to the best fit) plotted against the equivalent hydrogen column density of the Morrison & McCammon absorber (at $z = 0.524$) (beyond the fixed Galactic absorption at 7.6×10^{20} cm^{-2}) in the combined *ROSAT* and *ASCA* data. The fit required that the absorption is the same between *ASCA* and *ROSAT* but allowed for the power-law index and normalization to vary independently.

an absorbed broken power-law model, where we required that the absorption (assumed at $z = 0$), the break energy E_b, and both power-law indices α_{lo} and α_{hi} are the same for both data sets, but we allowed the normalization to be free. The resulting total χ^2 is 428 for 394 PHA channels, versus 371 if we adopt an absorbed power-law model with separate power-law indices for *ROSAT* and *ASCA* data. Thus, we conclude that a broken power-law model with a single set of parameters is *not* a better description of both *ROSAT* and *ASCA* data than simple power laws with separate indices. The fact that the absorption between the two data sets is quite similar further strengthens the fact that both continua are well described by simple power laws; if this were not the case, we would see a disagreement between the inferred values of N_H for the *ROSAT* and *ASCA* data. We note here that other forms of the "soft excess" (thermal bremsstrahlung or a black body) yielded similar results.

Nonetheless, since the *ROSAT* data show steeper spectrum than the *ASCA* data, the overall spectrum must have a "soft excess," but its contribution is strongly variable. Specifically, the break energy E_b, below which this "soft excess" dominates, must have shifted from somewhere *above* the *ROSAT* bandpass (>2 keV) during the *ROSAT* observation to *below* the *ASCA* bandpass (<0.5 keV) during the *ASCA* observation, such that the *ROSAT* data represent a nearly "pure" soft excess, while the *ASCA* data are nearly a "pure" hard power-law component. In fact, if the flux of the hard component were the same during the *ROSAT* observation as we measured it in the *ASCA* observation, we would have seen the break between the hard component and the "soft excess" at ~5 keV. Unfortunately, this is, of course, beyond the bandpass of the *ROSAT* PSPC.

Using both data sets simultaneously, we can further constrain the amount of absorption and tighten the confidence ranges on the two spectral indices. For this, we fitted jointly the *ROSAT* and full-bandpass *ASCA* data, allowing the index and normalization to be fitted independently, but requiring a common value of absorption for the two data sets. This procedure, of course, assumes that there was no change in absorption over 6 months, which is probably reasonable, given the confidence contours in Figure 4. First we adopted a simple absorbed power-law model. The best-fit parameters for the joint *ROSAT-ASCA* fit are $N_H = 2.8 \pm 0.4 \times 10^{21}$ cm^{-2}, $\alpha_{ROSAT} = 1.92^{+0.25}_{-0.27}$, and $\alpha_{ASCA} = 1.02 \pm 0.08$, with $\chi^2 = 371$ for 394 PHA bins. Similarly to the individual *ROSAT* and *ASCA* fits, we also attempted a model where we required that the excess absorption is as given by MMC83, at $z = 0.524$. This yielded $N_H(z = 0.524) = 4.2^{+0.9}_{-0.8} \times 10^{21}$ cm^{-2}, $\alpha_{ROSAT} = 1.77^{+0.25}_{-0.23}$, and $\alpha_{ASCA} = 0.93^{+0.08}_{-0.07}$, with $\chi^2 = 368$ for 394 PHA bins (see Fig. 5). We note here that while there is an improvement in χ^2 of 3, this provides only a very marginal evidence that the excess absorber is at $z = 0.524$. We note also that the *ROSAT* and *ASCA* data alone do not favor any particular redshift of the absorber ($\Delta\chi^2 < 2$ for any other redshift, as compared to $z = 0.524$).

4. DISCUSSION

4.1. *Excess Soft X-Ray Absorption*

4.1.1. *Origin of the Excess Absorption*

Both *ROSAT* and *ASCA* data sets show that the X-ray data for AO 0235+164 can be fitted well by a model with a power-law continuum and absorption, but the level of

© American Astronomical Society • Provided by the NASA Astrophysics Data System

1996ApJ...459..156M

absorption exceeds that expected from the H I column measurements in our Galaxy. Of the various origins for this, we consider the following: first, it could be caused by an excess in the ratio of X-ray column to H I in our own galaxy. This may be further divided into explanations arising from absorption by gas which does not show up as 21 cm emission, or which is on a length scale not resolvable by 21 cm maps, or by gas which is not hydrogen but which should be detectable in other ways. The other possibility we consider is that the gas is in the intervening galaxy.

The possibility that the excess absorber is, at least partially, in our Galaxy, in a form undetectable with the 21 cm technique, may be supported by the case of the extragalactic source, NRAO 140, in which there is a substantial amount of molecular gas in the line of sight. In this object, the molecular gas is measured in the ^{12}CO band (Bania, Marscher, & Barvainis 1991) and is contributing to X-ray absorption (Marscher 1988a; Turner et al. 1995). However, the galactic latitude of AO 0235+164 of $b = -39°$ makes this less likely than for NRAO 140, at $b = -19°$. The inspection of the ^{12}CO map in Dame et al. (1987) indicates no significant ^{12}CO emission at the location of AO 0235+164; however, the map resolution is modest. Under the premise that the diffuse Galactic 100 μm emission correlates well with the total (atomic and molecular) gas column density (Boulanger & Perault 1988), we also inspected the *IRAS* 100 μm map (Wheelock et al. 1994). We found that there is no significant (>20% in intensity) structure within 30′ of the position of AO 0235+164 and that the 100 μm surface brightness at the position of the source and its vicinity is $\sim$6.2 MJy sr^{-1}. Using the conversion of Boulanger & Perault (1988) of 0.85 MJy sr^{-1} per 1×10^{20} cm^{-2}, we obtain a value of 7.2×10^{20} cm^{-2}, in good agreement with the H I value, and thus the excess absorption is most likely extragalactic. We can probably discount the possibility that absorption is at or near $z = 0.94$, the redshift of the BL Lac object itself, as no corresponding absorption features are present in the high-resolution optical spectrum (Cohen et al. 1987). Since, as we argued above, the *IUE* data rule out a significant neutral H column density of the system at $z = 0.852$, we conclude that the excess absorption in AO 0235+164 is most likely caused by the system at $z = 0.524$; this is further supported by the substantially stronger Mg II absorption at $z = 0.524$ than at $z = 0.852$ (see, e.g., Wolfe & Wills 1977).

The soft X-ray absorption observed in the *ROSAT* and *ASCA* data is primarily attributable to helium, carbon, and oxygen. In the previous fits, we used a redshifted Morrison McCammon absorber, which assumes that the ratios of these elements to each other and to hydrogen are solar, and thus the fit value, even though parameterized as an equivalent hydrogen column density, is a measure of the column density of He, C, and O *at ratios fixed to each other*. This, of course, is probably incorrect; the elemental abundances in the $z = 0.524$ system are unlikely to be solar, and we discuss this below.

4.1.2. *Elemental Abundances in the z = 0.524 System*

The comparison of the optical and soft X-ray absorption against the 21 cm radio absorption in AO 0235+164 can, in principle, yield the measurement of elemental abundances relative to hydrogen in the intervening system. The use of the optical absorption lines is difficult because only a study of ionized species is possible, and the relative population of ionized-to-neutral species is not well known. Also, these lines are extremely narrow, and thus they are saturated, and it is necessary to revert to a curve-of-growth analysis. The X-ray route, which we attempt here, is more promising, but there are two important issues that have to be addressed: the first is the interpretation of the 21 cm measurements. There are no contemporaneous 21 cm and X-ray data, which adds to the uncertainty of such measurement if the absorption were variable, which is likely to be the case (see Wolfe et al. 1982). Furthermore, the determination of the 21 cm hydrogen column density in the intervening system is directly proportional to the hydrogen spin temperature T_S, which is poorly known. Nonetheless, there is at least a lower limit on T_S of 460 K (Briggs & Wolfe 1983), although Snijders et al. (1982), using the *IUE* UV data, argue that it is 140 K. Roberts et al. (1976) give the 21 cm absorbing column density $N_{\rm H\,I} \simeq 2.3 \times 10^{19} \times T_S$ cm^{-2}; with $T_S =$ 460 K, $N_{\rm H\,I} \simeq 10^{22}$ cm^{-2}.

The second issue arises from our inability to resolve the effects of absorption resulting from individual elements in our X-ray data via distinct absorption edges. In the fits presented in the previous sections, we made an assumption that the relative ratios of abundances of O to C to He in the $z = 0.524$ system are solar. While it allows for a convenient parameterization of the absorption, this assumption is probably not valid, and this affects our conclusions. This is because a part of the excess absorption observed by us is attributable to helium. While C and O are certainly chemically processed in stars, He only originates partially from stars but mainly from the big bang nucleosynthesis. Olive & Steigman (1995) report that the generally accepted value of the ^{4}He mass fraction Y_p is between 0.22 and 0.24, corresponding to the ratio by number to hydrogen $y_4^{\rm BBN}$ of 0.072 to 0.08. The commonly accepted solar value $y_4^{\rm Solar}$ is 0.1 (see MMC83), and thus the remainder, or the ratio (by number) of ^{4}He atoms produced by stellar and galactic chemical evolution to hydrogen atoms in the MMC83 absorber $y_4^{\rm Chem}$, is 0.024. This is very important in our study, since only 24% of He in the MMC83 absorber is "tied" to C and O via chemical evolution, and 76% is "tied" to hydrogen. As a result, instead of establishing the confidence limits on the absorption attributable to He, C, and O, we can only determine the limits on the processed elements modulo the combined column density of hydrogen and primordial helium. Of course we are making a (probably reasonable) assumption that the ratio of the *processed* He to O to C in the $z = 0.524$ system is solar, but this is one assumption we can currently test only crudely (see § 4.1.3).

We can measure such confidence limits by assuming that there are two separate absorbing columns in the $z = 0.524$ system: one "primordial," consisting of hydrogen plus 76% of He in the MMC83 absorber (which we denote as $N_{\rm H}^{\rm BBN}$), and the other "processed," consisting of no H, He at 24% of the MMC83 value, plus all heavier elements (which we denote as $N_{\rm H}^{\rm Chem}$); $N_{\rm H}^{\rm Chem}$, by design, as a solar ratio of the chemically reprocessed element heavier than He. We note that we assume that most of the He (as well as other absorbing elements) is not fully stripped, or else it would have no X-ray opacity. We fitted simultaneously the *ROSAT* and *ASCA* data to a power-law model, with three absorbers: absorption from our own Galaxy fixed at the 21 cm value, plus the two components of the $z = 0.524$ system as above, requiring that the absorption is common to the data from both instruments, but allowing the power-law spectral

© American Astronomical Society • Provided by the NASA Astrophysics Data System

1996ApJ...459..156M

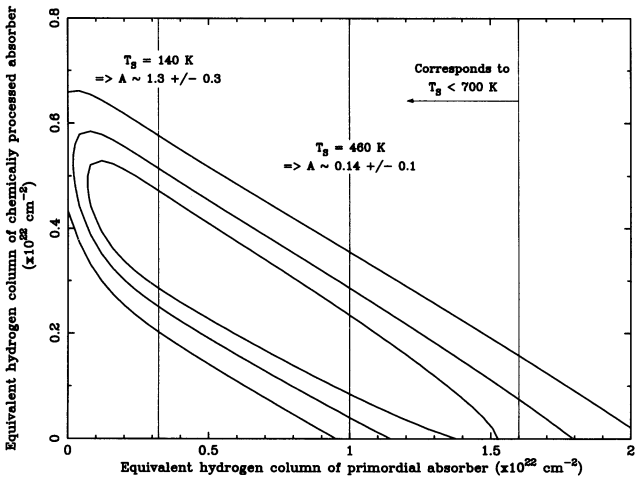

FIG. 6a

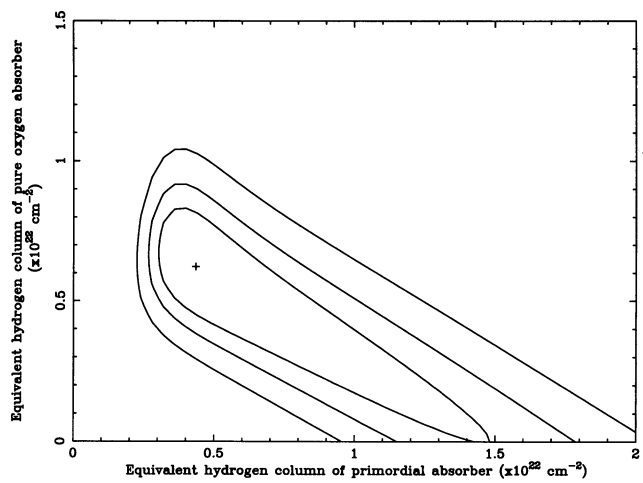

FIG. 6b

FIG. 6.—(*a*) Confidence regions ($\chi^2_{\rm min}$ + 2.3, 4.6, and 9.2) on the "primordial" absorber (with the primordial H to ^{4}He ratio) plotted against the "chemically processed" absorber (where the elemental abundances are solar *minus* the "primordial"). It is clear that the true hydrogen column density $N_{\rm H}$ cannot exceed 1.6×10^{22} cm^{-2}, as any admixture of reprocessed material would only reduce the absorbing column. This plus the redshifted 21 cm data of Roberts et al. (1976) yield the plotted upper limit on the spin temperature $T_S < 700$ K. Two vertical lines mark the column densities for $T_S = 460$ K (implying metallicity A of 0.14 ± 0.11 solar) and $T_S = 140$ K (implying metallicity A of 1.3 ± 0.3 solar). (*b*) Same as (*a*), but the vertical axis is the equivalent hydrogen column density of material consisting entirely of oxygen. The X-ray data allow up to $\sim 6 \times 10^{18}$ cm^{-2} of absorbing column of pure oxygen and are consistent with material entirely devoid of oxygen.

index to be fitted independently (see § 3.3). In Figure 6*a*, we plot the confidence contours of the "primordial" versus "processed" absorber, both parameterized as an equivalent hydrogen column density. As expected, the two parameters are correlated, but even at the unlikely zero value of the "processed" absorption, we cannot have more (at 90% confidence) than $N_{\rm H}^{\rm BBN}({\rm max}) \simeq 1.6 \times 10^{22}$ cm^{-2} of hydrogen absorption in the $z = 0.524$ system. This is very interesting, since via the constraint from the redshifted 21 cm data, we now can derive an upper limit on the spin temperature T_S in the $z = 0.524$ system to be less than $[N_{\rm H}^{\rm BBN}({\rm max})/2.3 \times 10^{19}$ cm^{-2}] K, or $T_S < 700$ K (see Fig. 6*a*). We note that if all He is primordial (as it is sometimes assumed), the limit on T_S becomes even tighter, by about 15%. Finally, it is apparent from this figure that we can establish the ratio of "processed" to "primordial" column densities A as a function of T_S; A is essentially the metallicity (as compared to solar) in the intervening system. If $T_S = 460$ K, then $A = 0.14 \pm 0.11$; if $T_S = 140$ K, then $A = 1.3 \pm 0.3$.

4.1.3. *Limits on Abundances of Individual Elements*

In principle, given data with better energy resolution and signal-to-noise ratio, we should be able to measure the depth of the C, O, Mg, and possibly Si K and Fe L edges (at their respective redshifted energies) separately, thus obtaining a direct measure of the column densities of these elements. C is redshifted out of the *ROSAT* bandpass; the modest energy resolution of *ROSAT* (where the O edge is) and limited statistics (where we could conceivably detect other edges) preclude such a measurement. The inspection of the data (see Figs. 2 and 3) reveals no obvious discrete absorption or emission features in the spectrum of the source. In fact, as we discussed above, our data allow an absorber that is pure hydrogen and helium (see Fig. 6*a*). Nonetheless, we can place some confidence limits on the absorbing column densities for some elements. To that end, we performed spectral fits to the *ROSAT* and *ASCA* data with a variable abundance absorber with only a given element present, placed at $z = 0.524$. As in the joint *ROSAT* + *ASCA* fits discussed in §§ 3.3 and 4.1.2, we fixed the Galactic absorption and allowed the spectral indices to vary independently, but we required the absorption to be the same for the two instruments. For O (and to a much lesser extent, for other elements) this is a "worst case" abundance limit, since an assumption that all the "processed" absorption is attributable to a single element requires larger columns than we really expect (compare Figs 6*a* and 6*b*).

The effects of carbon cannot be distinguished from these of He, since its K edge is redshifted even out of the *ROSAT* bandpass. Thus, we first consider oxygen; we separated the absorbing effect of it from other elements by allowing two separate absorbing columns, parameterized as equivalent neutral hydrogen column density. One was pure oxygen at the solar ratio of O to H, and the other was the "primordial" absorber as discussed above, containing H and 76% of the solar fraction of He. Our results are shown in Figure 6*b*, where we plot confidence contours of these absorbers. As expected, the two columns are anticorrelated, but importantly, we can limit the total equivalent hydrogen column of pure O absorber $N_{\rm H}^{\rm O} < 0.85 \times 10^{22}$ cm^{-2}, which corresponds to the a pure O column $N_{\rm O} < 6 \times 10^{18}$ cm^{-2}.

We performed similar fits for magnesium, iron (which are of particular interest, since the optical absorption lines in the $z = 0.524$ system are Mg II and Fe II), and silicon. The absorption from these heavier elements is not correlated with the "primordial" column, since their K edges are at higher energies than O, and thus *ASCA* data would be able to resolve them. Our data can limit the columns of Si and Fe to $N_{\rm H}^{\rm Si} < 0.9 \times 10^{22}$ cm^{-2}, corresponding to $N_{\rm Si} < 3.4 \times 10^{17}$ cm^{-2} and $N_{\rm H}^{\rm Fe} < 2.7 \times 10^{22}$ cm^{-2}, corresponding to $N_{\rm Fe} < 9 \times 10^{17}$ cm^{-2}. For magnesium, there is a marginal evidence of an edge in the data, but this is at less than 99% confidence; again, our limits for Mg are $N_{\rm H}^{\rm Mg} \sim 2.4 \pm 2.0 \times 10^{22}$ cm^{-2}, corresponding to $N_{\rm Mg}$ of $\sim 9.6 \pm 8.0 \times 10^{17}$ cm^{-2}. We note that a high-resolution X-ray spectroscopic observations (as, e.g., with the X-ray

© American Astronomical Society • Provided by the NASA Astrophysics Data System

1996ApJ...459..156M

Spectrometer planned to fly on *Astro-E*, or *Advanced X-Ray Astrophysics Facility* gratings), should yield the column densities of individual elements *directly* by resolving the individual edges.

4.1.4. *Possible Variability of Absorption and its Implications*

The level of soft X-ray absorption inferred from the *ROSAT* and *ASCA* data is substantially lower than that measured in 1980 with the *Einstein Observatory* IPC, which corresponds to an excess (at $z = 0.524$) of $1.9^{+3.6}_{-1.4} \times 10^{22}$ cm^{-2} (Madejski 1994). This difference can be a result of the residual calibration uncertainties of the IPC, but, given the variability of the redshifted 21 cm absorption by as much as a factor of 2 (Wolfe et al. 1982), the variability of the X-ray absorption is likely. Similar change in absorption, probably arising from a passage of a molecular cloud in our own Galaxy through the line of sight, has been observed in the OVV quasar NRAO 140 (Marscher 1988b; Turner et al. 1995). In the IPC data for AO 0235+164, the errors on both the asorption and spectral index separately are large, but these fit parameters are correlated (see Figs. 2 and 3 in Madejski 1994). The flux level of the object during the *Einstein* observation was comparable to the mean *ROSAT* flux, and thus the index in the IPC data was likely to be comparable to the *ROSAT* value. If this was the case, the errors in the IPC data are much smaller, and the difference in the excess absorption between the epochs of the IPC and the *ROSAT*/*ASCA* observations must have been $\sim 10^{22}$ cm^{-2}.

While the evidence of the absorption variability is only tentative, it is worth considering the implications if it is real. In the reference to the variability of the 21 cm absorption, Wolfe et al. (1982) point out that either the source of the background radiation (in our case of X-rays) moved slightly, appearing from behind a partially absorbing cloud, or the absorber moved across the line of sight to a steady source. With the superluminal expansion observed in many compact radio sources, the first possibility is not unlikely; even a tenth of a milliarcsecond of motion of an X-ray source would correspond to sampling a path shifted by ~ 1 pc at $z = 0.524$, which is certainly comparable to a size of molecular cloud structures. However, this would imply as yet unobserved change of the spatial structure of the X-ray–emitting region. The other option is a transverse motion of an absorbing cloud across the line of sight in the intervening system. At $z = 0.524$, such a cloud would have to have a column density equal to the difference of the IPC and *ROSAT*/*ASCA* columns, or $\sim 10^{22}$ cm^{-2}. A reasonable transverse velocity of such a cloud could be 200 km s^{-1} or less; the maximum distance traveled by such a cloud over ~ 15 yr would be then $\sim 2 \times 10^7$ cm s^{-1} $\times$ $\sim 5 \times 10^8$ s $\simeq 10^{16}$ cm. Under the simplest symmetry assumptions, this would imply the density on the order of $\sim 10^6$ H atoms cm^{-3} and total content of $\sim 4 \times 10^{54}$ H atoms, corresponding to $\sim 6 \times 10^{30}$ g, which is not unreasonable; comparable structures within a galaxy are cores of molecular clouds, although the filling factor of such clouds is not large. Of course, the X-ray absorption technique is not the only means to study such structures; high-resolution absorption studies against AO 0235+164 or NRAO 140 in ^{12}CO could provide additional information.

Further refinement of the determination of the nature of the intervening absorber will be accomplished via future optical/UV spectroscopy. That is because both H Lyα and the H Lymann edge of the material in the $z = 0.524$ system are longward of the Galactic H Lyman edge, and thus a careful determination of the $z = 0.524$ edge depth will provide the definitive answer as to the column density of hydrogen atoms. A *Hubble Space Telescope* observation of this object is already planned (R. Cohen, private communication), but it is postponed until the object is brighter than the current level ($m_v \sim 19$). In addition to the measurement of discrete spectral features, such UV data will provide information as to the dust content of the intervening system, which is likely to be significant, judging by the steep *IUE* spectrum with α of 3.5 ± 0.5 (Snijders et al. 1982) and red optical colors (Rieke et al. 1976). To that end, it would be particularly advantageous to obtain simultaneous X-ray spectroscopy, allowing an extrapolation of the UV continuum to the energies beyond which it is affected by the Galactic (and the intervening) absorption; an additional benefit would be an ability to measure the gas-to-dust ratio in the intervening system.

4.2. *X-Ray Continuum*

We observed AO 0235+164 in the X-ray band on two occasions: when it was bright, soft ($\alpha \sim 2$), and highly variable, and ~ 6 months later, when it was fainter, harder ($\alpha \sim 1$), and relatively constant. This behavior of the X-ray continuum is almost exactly the opposite of what has been observed with *Ginga* in other BL Lac objects (see Tashiro 1992). In the case of PKS 2155−304, perhaps the most extensively observed BL Lac object in the X-ray band, the *Ginga* observation revealed that the spectrum hardened when the source got brighter, and then, in the course of becoming fainter, it also became steeper (Sembay et al. 1993). This happened on a relatively short timescale, on the order of several hours, but such behavior is also consistent with the variability observed at other epochs. This fits well into the synchrotron model for X-ray emission, where the spectrum steepens as a result of the decreasing lifetime of the radiating particles with increasing energy, as is expected in the case of synchrotron cooling. However, such a model also implies very low magnetic fields and extreme Lorentz factors of the emitting electrons (Tashiro 1992; Tashiro et al. 1995). Alternatively, such a behavior can also be explained in terms of an inhomogeneous model without the necessity of involving extreme parameters of emitting regions. In such a model, the fastest and highest amplitude variability is produced by the innermost parts of a jet. Since in this model, the high-energy cutoffs of synchrotron radiation spectra drop with distance (Ghisellini & Maraschi 1989), we can expect that soft X-rays, which form the high-energy tail of the synchrotron component, arise from the innermost parts of a jet. At lower frequencies, the contribution from larger distances dominates, and the variability timescale, if related to propagating disturbances or shocks, is correspondingly longer.

The spectral behavior of AO 0235+164 does not fit into such a pattern: instead, its continuum is hard when it is faint. This is in disagreement with a simple synchrotron model as the sole description of X-ray emission in all of our observations. We are driven to a conclusion that we observe two separate spectral components, where the drop in the intensity of the soft component uncovers the hard component. This interpretation, of course, makes a strong prediction, where in the intermediate flux states, the X-ray spectrum of this object is likely to show simultaneously both the hard component dominating the *ASCA* data as

© American Astronomical Society • Provided by the NASA Astrophysics Data System

1996ApJ...459..156M

well as a discernible "soft excess" of the component dominating the *ROSAT* data.

As to the origin of the soft ($\alpha \sim 2$) component of the X-ray emission, there is circumstantial evidence that in AO 0235+164 we observe the high-energy tail of the electron distribution radiating via the synchrotron process. As we mentioned above, this is most likely to be the case in PKS 2155−304. Further support is from the correlated optical, UV (*IUE*), and X-ray variability (Edelson et al. 1995; Brinkman et al. 1994), and for less well studied objects, from the location of the X-ray spectrum on the extension of the UV power law (see Tashiro 1992; Madejski 1985).

What is the origin of the hard X-ray spectrum in AO 0235+164? The discovery of GeV γ-ray emission from the blazar 3C 279 (Hartman et al. 1992), and subsequently from $\sim$40 other flat-spectrum compact extragalactic radio sources (see, e.g., Fichtel et al. 1994; von Montigny et al. 1995) established these objects as a class of GeV emitters, of which AO 0235+164 is a member. A plausible explanation of the mechanism responsible for the GeV emission in these sources is Comptonization, and the faint, hard X-ray emission could be the onset of the Compton component. It is interesting to note here that the interpretation of hard X-ray radiation as arising from Comptonization fits well the *Ginga* observations of radio flat spectrum quasars, but not of BL Lac objects (Kii et al. 1992), at least not of the X-ray selected ones. There are several classical, radio-selected BL Lac objects, where the relationship of the X-ray spectrum, which is hard, and *not* on the extrapolation of the optical-UV slope, suggests the Compton process as the origin of X-rays (see, e.g., another faint EGRET-detected BL Lac object PKS 0735+178, with $\alpha_X \sim 0.7$; Bregman et al. 1984, Madejski & Schwartz 1988). The *ASCA* X-ray spectrum of AO 0235+164 appears similar to that of PKS 0735+178, and thus it is suggestive that the signature of the Compton emission in X-rays is more likely to be observed in the radio-selected BL Lac objects.

A more detailed study of this putative Compton component may be aided by a comparison of our simultaneous X-ray–γ-ray data to those obtained in the 1993 campaign for the blazar 3C 279 (Maraschi et al. 1994). It is likely that both objects were observed in their respective "low states," since in both bases, the levels of X-ray and γ-ray emission were amongst the lowest observed. For 3C 279, the ratio of the 1 GeV to 1 keV flux per logarithmic frequency interval [in $E \times F(E)$] was roughly 8, whereas for AO 0235+164, we observe the ratio of $\sim$30 (see Fig. 7). This is in contrast to the 1 GeV to 1 keV flux ratio of $\sim$100 in the high state for 3C 279; unfortunately, we do not have information about such ratio during high γ-ray state for AO 0235+164.

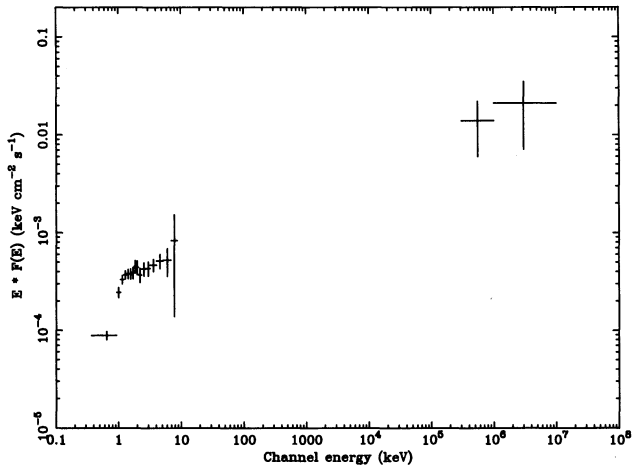

FIG. 7.—Simultaneous X-ray to γ-ray $E \times F(E)$ spectrum of AO 0235+164 obtained in 1994 February. The X-ray data are plotted as observed, i.e., including the effects of absorption. Note that the source was detected in each of the plotted EGRET spectral bands only at 2–3 σ, but the plot is meant to illustrate that the source spectrum is consistent with a power-law model with $\alpha = 1$, previously reported by Hunter et al. (1993).

4.3. *Overall Electromagnetic Emission*

There is very good evidence that the overall electromagnetic emission in blazars is anisotropic, Doppler-boosted (beamed) toward the observer, and in reality, the monochromatic luminosity inferred under an assumption of isotropy must be reduced by a factor of $\delta^{-(k+\alpha)}$, where $k = 3$ is for a relativistically moving cloud of emitting gas, and $k = 2$ is for a steady state jet, and α is the energy spectral index. [Here δ is defined in the standard way as $\Gamma^{-1}(1 - \beta \cos \phi)^{-1}$, where Γ is the Lorentz factor of the jet, $\beta = v/c$, and ϕ is the angle to the line of sight.) In the radio regime, the evidence comes from superluminal expansion, observed with the VLBI. In the optical and UV, there is no irrefutable evidence for beaming, but the extremely rapid, large-amplitude variability and high polarization would require extreme conditions without beaming (Blandford & Königl 1979). Finally, relativistic beaming is required in order to avoid absorption of GeV photons by X-ray photons in the pair production process (see, e.g., Maraschi, Ghisellini, & Celotti 1992).

Taking into account that absorption of γ-ray photons with energy E_γ is dominated by X-rays with energy E_X given by $E_\gamma(1 + z)/\delta \times E_X(1 + z)/\delta \sim (m_e c^2)^2$ (where E_γ and E_X are photon energies as measured by observer located at $\phi \leq 1/\Gamma$), the X-ray radiation field opacity for γ-rays at $E_\gamma \geq 1$ GeV for nonrelativistic jet ($\Gamma \sim 1$) is determined by compactness of radiation field in the soft X-ray band ($E_X \leq 1$ keV). Since for many blazars the X-ray compactness, as determined from the ratio of the X-ray luminosity variability magnitude to the variability timescale ($\Delta L_X/\Delta t$), gives optical thickness for pair production $\tau_{\gamma\gamma} \gg 1$, the observed transparency of the source for γ-rays up to GeV energies can be achieved only if $\delta \geq$ few. Assuming that the γ-rays and soft X-rays from AO 0235+164 are produced in the same region, we can calculate opacity for pair production from *ROSAT* data. Using formula given by equation (3) in Mattox et al. (1993), but corrected for the error,[7] we fnd that for nonrelativistic outflow ($\Gamma \sim 1$) and the parameters observed in AO 0235+164 ($z = 0.94$, $\alpha = 2$, $T = 3$ days, and $F_{keV} = 2.5$ μJy), the opacity for 1 GeV photons would be $\tau_{\gamma\gamma} \sim 0.8 \times 10^4$, and $\delta > 3.1$ is required in order to have $\tau_{\gamma\gamma}(E_\gamma > 1\ \mathrm{GeV}) < 1$.

Strictly speaking, the above $\tau_{\gamma\gamma}$ argument for anisotropy only applies if the γ-ray–emitting region is the same as the soft X-ray–emitting region and, for now, we do not have any clear observational indications that this is the case. This

[7] In eq. (3) in Mattox et al. (1993), the factor $(1 + z)$ should have power (2α) rather than $(4 + 2\alpha)$. The error is a consequence of using the wrong formula for the source frame differential luminosity. In an unnumbered equation three lines before eq. (2), the factor $(1 + z)^3$ is correct only if followed by square of angular diameter distance which is $D_\phi = D_L/(1 + z)^2$. Therefore, in formulae (2) and (3) the factor $(1 + z)$ should have power (2α), and in eq. (4) the factor $(1 + z)$ should have power $-(2\alpha)$. The same error is followed in the paper by von Montigny et al. (1995) in eqs. (5) and (6).

© American Astronomical Society • Provided by the NASA Astrophysics Data System

1996ApJ...459..156M

is important, since the jets are likely to be inhomogeneous. However, since in some blazars the γ-ray variability is noted on timescales as short as a few days (Kniffen et al. 1993; von Montigny et al. 1995), and because γ-ray emission is accompanied by X-ray emission of the same population of relativistic particles, for such sources $\delta >$ a few can be deduced as well (note that X-rays produced in the γ-ray emission region can dominate the X-ray radiation field compactness locally, even if the observed X-rays are dominated by other jet regions).

While it is reasonably well established that the radio-through-UV (and in many cases, soft X-ray radiation) in blazars arises from the synchrotron process in a jet or plasma clouds moving at relativistic speed, the location and the details of the mechanism responsible for the X-ray–to–γ-ray portion of the spectrum is still under some debate. The most common family of models invoked to explain the strong GeV emission in blazars involves Comptonization of lower energy photons, and it is likely that the faint, hard X-ray emission observed by us with *ASCA* is the low-energy end of the Compton component. In the two general classes of models, the seed photons for Comptonization are either produced by external radiation sources (the external radiation Compton, or ERC models), or internally via the synchrotron process (the so-called synchrotron self-Compton, or SSC, models).

The ERC models rely either on the UV radiation from the central source, e.g., from the accretion disk around the central regine (Dermer, Schlickeiser, & Mastichiadis 1992), or radiation that is produced by scattering and reprocessing of the central radiation by emission-line clouds and the intercloud medium (Blandford 1993; Sikora, Begelman, & Rees 1994). However, at least for the latter model, BL Lac objects are generally devoid of emission lines, and thus the scattering would have to happen on some hot ambient medium, existence of which cannot be proved directly by observations. The SSC models explain the γ-ray emission as resulting from Comptonization of synchrotron radiation, where both Compton and synchrotron radiation are produced by the same population of relativistic electrons/positrons accelerated locally within a relativistic jet (Rees 1967; Königl 1981; Marscher & Gear 1985; Ghisellini & Maraschi 1989).

Both the SSC and ERC models were recently invoked to describe the multiwavelength data for the blazar 3C 279 (Maraschi et al. 1994). One successful variant of the SSC model, capable of explaining the variability patterns in the radio, IR, optical, UV and X-ray bands, was proposed by Maraschi et al. (1992). In this model, the highest energy synchrotron photons, i.e., UV and in BL Lac objects soft X-rays, and the highest energy Compton photons, i.e., GeV γ-rays, are produced in the innermost parts of the jet. This model predicts the largest variability of the Compton component in γ-rays and the largest variability of the synchrotron radiation in UV or soft X-rays. The model seems to be in qualitative agreement with the multiwavelength and multiepoch observations of the blazar 3C 279 (Maraschi et al. 1994). However, as was noted by these authors, the ERC model with variable Γ can fit these data as well.

The SSC interpretation of γ-ray production in AO 0235+164 may, at a first glance, be challenged by the fact that the fast variability in the soft X-ray band is not accompanied by variability in γ-rays. However, we can expect that synchrotron high-energy tail, observed in soft X-ray band, is produced by the same particles that are responsible for the production of the Compton high-energy tail at $E_\gamma > 1$ GeV, which is too weak to be detected during the low state (when the observed X-rays are dominated by the Compton component).

4.4. *Comparison of AO 0235+164 to X-Ray–selected BL Lac Objects*

It is interesting to compare the X-ray and γ-ray properties of classical, radio-selected BL Lac objects to these selected or classified on the basis of their X-ray emission (for the discussion of the two subclasses of BL Lac objects, see, e.g., Stocke et al. 1989; Giommi et al. 1990). In general, relatively few BL Lac objects as compared to OVV quasars have been detected in the GeV energies. Admittedly, selection criteria are not very rigorous, but, while the X-ray surveys continue to reveal new objects, the detection of GeV γ-rays in X-ray–selected BL Lac objects is restricted to two objects. One is Mrk 421, which shows consistently only a modest GeV flux, despite the relative proximity (see Lin et al. 1992; Fichtel et al. 1994). The other is PKS 2155−304, only recently detected by EGRET at a fairly faint level (Vestrand, Stacy, & Sreekumar 1995). It is interesting to compare the 1 GeV to 1 keV flux ratios of X-ray–selected BL Lac objects from the Piccinotti survey (Mrk 421, PKS 0548−322, PKS 2155−304, Mrk 501, and 1218+304) to that measured by us for AO 0235+164. Both PKS 2155−304 (Vestrand et al. 1995) and Mrk 421 (Lin et al. 1992) are detected at a faint level; the remaining three have published GeV upper limits (Fichtel et al. 1994). We list these, together with 1 keV flux

TABLE 3

COMPARISON OF THE RATIO OF 1 GeV TO 1 keV FLUXES FOR AO 0235+164 AND X-RAY–SELECTED BL LAC OBJECTS

OBJECT NAME	FLUX DENSITY (mJy)			AVERAGE 1 keV FLUX density (Jy × Hz)	EGRET > 100 MeV PHOTON FLUX (×10 E−7 photons FLUX cm^{-2} s^{-1})	1 GeV FLUX DENSITY (Jy × Hz)	1 GeV/1 keV Flux Ratio
	Einstein	*EXOSAT*	*ASCA*				
AO 0235+164.....	...	...	0.3	7.44E+10	1.4	2.2E+12	30
X-ray–selected BL Lac objects:							
PKS 0548−322.....	9.0	5.9	...	1.79E+12	<0.8	<1.3E+12	<0.70
1218+304	4.4	8.5	...	1.55E+12	<0.6	<9.4E+11	<0.6
Mrk 501	23.7	13.8	...	4.50E+12	<0.8	<1.3E+12	<0.28
Mrk 421	2.0	13.8	...	1.90E+12	2.1	3.3E+12	1.7
PKS 2155−304.....	29.0	28.5	...	6.90E+12	2.7	4.2E+12	0.61

NOTES.—*Einstein* fluxes from Madejski et al. 1991; *EXOSAT* fluxes from Sambruna et al. 1994; EGRET flux for PKS 2155−304 from Vestrand et al. 1995; other EGRET fluxes and upper limits for the X-ray–selected objects from Fichtel et al. 1994. The data for the X-ray–selected objects are not simultaneous with the EGRET data.

© American Astronomical Society • Provided by the NASA Astrophysics Data System

1996ApJ...459..156M

densities, in Table 3. To arrive at the 1 GeV flux upper limits, we use the same conversion of the photon count rate to 1 GeV flux density as for AO 0235+164 [which, with an assumed $\alpha = 1$, is 1×10^{-7} photons (>100 MeV) cm^{-2} s^{-1} = 1.6×10^{12} Jy × Hz].

It is appparent from Table 3 that the ratio of the observed 1 GeV flux densities (or upper limits) to these measured at 1 keV is substantially lower in the X-ray–selected BL Lac objects than we observe in AO 0235+164. We acknowledge that the X-ray data for these objects are not simultaneous with the GeV observations, but, given the multiple EGRET pointings at the regions of the sky at which these objects are located, the difference is likely real. This difference may be explained by the recent finding by Padovani & Giommi (1995), who note that the peak of the overall radio–through–X-ray flux distribution [in $E \times F(E)$] in X-ray–selected BL Lac objects is shifted toward higher frequencies, $\sim 10^{15}$–10^{16} Hz, as compared to $\sim 10^{13}$–10^{14} Hz for the radio-selected objects. In this scenario, in the X-ray–selected objects, the tail of the synchrotron emission dominates the soft X-ray spectrum and makes the contribution of the Compton radiation, if present at all, undetectable, in contrast to the radio-selected BL Lac objects, as AO 0235+164, where emission from *both* processes has been observed. If this is the case, a more meaningful comparison would be the ratio of the *peak of the synchrotron emission to the peak of the γ-ray emission.* In any case, there appears to be a clear conclusion: *selecting BL Lac objects via X-ray techniques does not lead to selection of the brightest γ-ray–emitting BL Lac, objects.*

5. CONCLUSIONS

We observed the BL Lac object AO 0235+164 with *ROSAT*, and then 6 months later simultaneously with *ASCA* and *CGRO* EGRET. Our observations revealed the following:

1. *ROSAT* data show that AO 0235+164 is rapidly variable in X-rays, with a rapid (<4 days) rise and a more gradual decay. No variability is observed in the *ASCA* or EGRET data.

2. The comparison of *ROSAT* and *ASCA* observations shows strong spectral variability in X-rays, with a change of the energy power-law index from ~ 2 in *ROSAT* data to ~ 1 in *ASCA* data (when the source was fainter). We interpret this as a signature of the steep tail of the electron distribution radiating via synchrotron emission dominating the higher flux *ROSAT* observation, and the fainter, harder Compton emission dominating the *ASCA* observation.

3. The excess absorption reported on the basis on the *Einstein* IPC data in this object is real, but it is currently less than the 1980 IPC data imply. Owing to the instrumental uncertainties of the *Einstein* IPC, we consider the variability of the absorbing column as only tentative. The *ROSAT* PSPC and *ASCA* data are in close agreement with each other on the column density of the absorber; under an assumption that it is at $z = 0$, it is $\sim 2.2 \times 10^{21}$ cm^{-2} equivalent H atoms above the Galactic value. The statistical quality of the X-ray data does not allow us to determine the location of the absorber; independently, the *IRAS* 100 μm data support the hypothesis that the excess absorption is not in Galaxy. Given the *IUE* observations of Snijders et al. (1982), we conclude that this absorber is from the intervening galaxy at the redshift of 0.524 and is the same material which is observed in the optical and radio, with a corresponding X-ray column of the Morrison & McCammon (1983) absorber (i.e., at the solar ratio of elements) of 4.2×10^{21} equivalent H atoms cm^{-2}.

4. Even in the unlikely case that the absorption observed by us in the $z = 0.524$ system arises from primordial helium, the comparison of the X-ray absorption to the 21 cm radio absorption limits the hydrogen spin temperature T_S to less than 700 K. The knowledge of T_S via independent means will enable a measurement of the abundances A of chemically processed elements in this system (as compared to hydrogen, and as a fraction of the solar value); assuming the ratio of chemically processed elements to each other to be solar, at $T_S = 460$ K, A is $\sim 0.14 \pm 0.11$; at $T_S = 140$ K, A is $\sim 1.3 \pm 0.3$.

5. Simultaneous *ASCA*-EGRET observation of AO 0235+164 shows that the $E \times F(E)$ at 1 GeV is about 30 times the X-ray (1 keV) $E \times F(E)$; this value is nearly 4 times greater than the ratio of GeV to X-rays for 3C 279 in the low state. This factor of 30 is also *very* substantially greater than for X-ray–selected BL Lac objects, where, for instance, a value of 0.6 is inferred for PKS 2155−304, suggesting important differences in the structure or orientation of the beamed emission between the two subclasses of BL Lac objects.

We are grateful to Steve Snowden for the help with the access and interpretation of the *IRAS* data, Professor John Stocke for discussions on taxonomy of BL Lac objects, Professor John Bally and Richard Mushotzky for discussions on the nature of the intervening absorber, the referee, Professor Thierry Courvoisier, for suggestions resulting in a clarification of some points in the paper, and Professor Mitch Begelman for many useful comments on the manuscript and hospitality at the University of Colorado. This research was supported by the Grants-in-Aid by the Ministry of Education, Culture, and Science (Monbusho) of Japan (05242101), and by NASA, via *GRO* grant NAG 5-2439, and *ROSAT* and *ASCA* observing grants.

REFERENCES

Abraham, R. G., Crawford, C. S., Merrifield, M., Hutchings, J. B., & McHardy, I. 1993, ApJ, 415, 101
Bania, T. M., Marscher, A. P., & Barvainis, R. 1991, AJ, 101, 2147
Blandford, R. D. 1993, in AIP Conf. Proc. 280, First CGRO Symp., ed. M. Friedlander, N. Gehrels, & D. J. Macomb (New York: AIP), 533
Blandford, R. D., & Königl, 1979, 232, 34
Boulanger, F., & Perault, M. 1988, ApJ, 330, 964
Bregman, J., et al. 1984, ApJ, 276, 454
Briggs, F. H., & Wolfe, A. M. 1983, ApJ, 268, 76
Brinkman, W., et al. 1994, A&A, 288, 433
Burbidge, E. M., Caldwell, R. D., Smith, H. E., Liebert, J., & Spinrad, H. 1976, ApJ, 205, L117
Cohen, R. D., Smith, H. E., Junkkarinen, V. T., & Burbidge, E. M. 1987, ApJ, 318, 577
Dame, T. M., et al. 1987, ApJ, 322, 706
Dermer, C., Schlickheiser, R., & Mastichiadis, A. 1992, A&A, 256, L27
Edelson, R., et al. 1995, ApJ, 438, 120
Elvis, M., Lockman, F. J., & Wilkes, B. 1989, AJ, 97, 777
Fichtel, C. E., et al. 1994, ApJS, 94, 551
Ghisellini, G., & Maraschi, L., 1989, ApJ, 340, 181
Giommi, P., Barr, P., Garilli, B., Maccagni, D., & Pollock, A. M. T. 1990, ApJ, 356, 432
Hartman, R., et al. 1992, ApJ, 385, L1
Hunter, S., et al. 1993, A&A, 272, 59
Kii, T., et al. 1992, in Frontiers of X-Ray Astronomy, ed. Y. Tanaka & K. Koyama (Tokyo: Universal Academy Press), 577
Kniffen, D. A., et al. 1993, ApJ, 411, 133
Königl, A. 1981, ApJ, 243, 700

© American Astronomical Society • Provided by the NASA Astrophysics Data System

1996ApJ...459..156M

Lin, Y. C., et al. 1992, ApJ, 401, L61
Madejski, G. M. 1985, Ph.D. thesis, Harvard Univ.
———. 1994, ApJ, 432, 554
Madejski, G. M., Mushotzky, R. F., Weaver, K. A., Arnaud, K. A., & Urry, C. M. 1991, ApJ, 370, 198
Madejski, G. M., & Schwartz, D. A. 1988, ApJ, 330, 776
Maraschi, L., Ghisellini, G., & Celotti, A. 1992, ApJ, 397, L5
Maraschi, L., et al. 1994, ApJ, 435, L91
Marscher, A. 1988a, ApJ, 334, 552
———. 1988b, in The Impact of VLBI on Astrophysics and Geophysics, ed. M. J. Reid & J. M. Moran (Dordrecht: Reidel), 35
Marscher, A. P., & Gear, W. K. 1985, ApJ, 298, 114
Mattox, J. R., et al. 1993, ApJ, 410, 609
Morrison, R., & McCammon, D. 1983, ApJ, 270, 119 (MMC83)
Olive, K. A., & Steigman, G. 1995, ApJS, 97, 49
Ostriker, J. P., & Vietri, M. 1985, Nature, 318, 446
Padovani, P., & Giommi, P. 1995, ApJ, 444, 567
Rees, M. J. 1967, MNRAS, 137, 429
Rieke, G. H., Grasdalen, G. L., Kinman, T. D., Hintzen, P., Wills, B. J., & Wills, D. 1976, Nature, 260, 754
Roberts, M. S., Brown, R. L., Brundage, W. D., Rots, A. H., Haynes, M. P., & Wolfe, A. M. 1976, AJ, 81, 293
Sambruna, R., Barr, P., Giommi, P., Maraschi, L., Tagliaferri, G., & Treves, A. 1994, ApJ, 434, 468
Sembay, S., et al. 1993, ApJ, 404, 112
Sikora, M., Begelman, M., & Rees, M. 1994, ApJ, 421, 153
Snijders, M. A. J., Boksenberg, A., Penston, M. V., & Sargent, W. L. W. 1982, MNRAS, 201, 801
Spinrad, H., & Smith, H. 1975, ApJ, 201, 275
Stocke, J. T., Morris, S. M., Gioia, I. M., Maccacaro, T., Schild, R. E., & Wolter, A. 1989, in BL Lac Objects, eds. L. Maraschi, T. Maccacaro, & M.-H. Ulrich (Berlin: Springer-Verlag), 242
Tashiro, M. 1992, Ph.D. thesis, Univ. Tokyo
Tashiro, M., Makishima, K., Ohashi, T., Inda-Koide, M., Yamashita, A., Mihara, T., & Kohmura, Y. 1995, PASJ, 47(2), 131
Turner, T. J., George, I. M., Madejski, G. M., Kitamoto, S., & Suzuki, T. 1995, ApJ, 445, 660
Vestrand, W. T., Stacy, J. G., & Sreekumar, P. 1995, IAU Circ, No. 6169
von Montigny, C., et al. 1995, ApJ, 440, 525
Wheelock, S.-L., et al. 1994, IRAS Sky Survey Atlas JPL Publication 94-11 (Pasadena: JPL)
Wolfe, A. M., & Wills, B. 1977, ApJ, 218, 39
Wolfe, A. M., Davis, M. M., & Briggs, F. H. 1982, ApJ, 259, 495

© American Astronomical Society • Provided by the NASA Astrophysics Data System